Inference of lumen area and PWV in a healthy adult thoracic aortic network using PINNs

[1]Javier Orera*, [1]Javier Murillo;

[1]Aragon Institute of Engineering Research, University of Zaragoza, Zaragoza, Spain

Keywords: 1D modelling, PINNs, lumen area, PWV, inference, aorta

Abstract. The reservoir function of the aorta refers to the mechanical compliance of the vessel wall, while the conduit function is related to the pressure differences along the vessel. These two aortic properties can be analysed using the time-domain, one-dimensional (1D) equations of blood flow in compliant vessels. Clinical measurements that personalize the geometry using Magnetic Resonance Imaging (MRI), aortic inflow and outflow boundary conditions of the computational framework, material properties as the Pulse Wave Velocity (PWV), as well as diastolic and systolic pressure at one point of the arterial network (using sphygmomanometry or tonometry) are required to calibrate the entire model. Another approach to evaluate the reservoir and conduit functions is to use time-varying cross-sectional averaged velocity in the lumen area, where this area is segmented only once along the aortic centreline at the flow peak-systolic time [1]. Using this latter approach, the objective of this work is to retrieve the evolution of aortic lumen area in time and space, including diastolic area, as well as space-varying PWV by means of Physics-Informed Neural Networks (PINNs) constrained with a haemodynamic model and trained with in-silico velocity data. We rely on a geometric segmentation of the thoracic aorta network composed of ascending aorta, aortic arch, upper cerebral branches and mid-lower thoracic descending aorta, and use PINNs in a piece-wise fashion to comply with fluid conservation laws at every individual major branch. Finally, we compare our results with MRI measurements of time-varying lumen area performed in a healthy adult and discuss the modelling assumptions on PWV proposed in [1].

1. Introduction

Over the past two decades, 1D cardiovascular simulators have gained important traction in the field of biomedical research for their low computational expenses and high speed [1]. As opposed to 3D models, which can only target a specific zone of the cardio-vasculature, 1D models offer the possibility to capture the main features of flow and pressure wave propagation across a high number of vessels (in the order of hundreds to thousands), both arteries and veins. Furthermore, coupling of the 1D wave propagation model with external boundary conditions, such as vascular beds (organs with high capillarity), whole-heart models, etc, is possible, leading to a closed-loop model that includes both arterial and venous circulation. From there, studies related to autoregulation of flow or body postural changes are possible [5].

One of the caveats that 1D cardiovascular simulator often face is the large number of parameters that have to be calibrated usually on the basis of noisy and sparse data, leading to an *inverse* parameter identification problem. These unknown parameters often relate to the geometry of the network of vessels and the vessel's stiffness, usually referred to in terms of Pulse Wave Velocity (PWV). If no measurement data of these is available, one possible approach is to use rough estimates that comply with literature measurements. If some measurements are available, a second approach is to extract these parameters using ad-hoc algorithms, such as the Time-to-Foot (TTF). However, if these parameters vary in time or space, their data-driven calibration requires the use of inverse solvers that embed both the physics of the flow as well as the fluid-wall interaction.

In this work, we focus on the intrathoracic aortic network, composed of ascending aorta (AA), upper cerebral branches (brachiocephalic artery (BCA), left common carotid artery (LCCA) and left subclavian artery (LSA)) and mid-lower thoracic descending aorta (DA). Current measurement procedures for measuring flow in the intrathoracic cavity are limited to 4D-MRI flow combined with angiography, and Doppler Ultrasound. Depending on the details of the procedure and the clinical device available, the resulting measurements include either (a) densely sampled velocity field along the aortic centreline, together with luminal area at several locations along the aortic centreline, where this area can exclusively be segmented at peak-systole time, as

exposed in [2], or (b) volume flow rate and area in time at several (often sparse and very specific) aortic locations, aortic geometry at the beginning of the diastolic phase, and additionally mean flow distribution in supra-aortic (upper) branches and pressure in the left carotid artery (via tonometry) [1]. Since in this work a 1D formulation is used, postprocessing involves averaging of the flow rate and area measurements over the cross section.

Given these variety across different clinical measurements under different clinical scenarios, the preferred inverse solver should be able to seamlessly integrate incomplete noisy and sparse data corresponding to any of the variables involved in the model, across the computational domain and its boundaries. Physics-Informed Neural Networks [3] (PINNs) offer the possibility to easily assimilate clinical data, together with fluid conservation laws and constitutive (closure) equations for the fluid-wall interaction, to provide accurate estimates of the parameters of interest.

First, we use PINNs to reconstruct the space-time evolution of the luminal area in a thoracic aortic network, given in-silico cross-sectional averaged velocity data and luminal area sampled exclusively at peak-systolic time, along the aortic centreline. No other boundary data on the luminal area is available, hence this leads to an ill-posed inverse problem with incomplete data, as described in (a). As a result, the algorithm is able to recover also the diastolic value of the luminal area in all vessels, that is, the unstressed geometry of the aortic network. Secondly, using the reconstructed geometry, we use a second PINN to infer the pressure field as well as the space-varying arterial stiffness, given a reference systolic and diastolic value of the pressure.

2. Methods

1D blood flow models are able to represent flow and pressure waves in compliant vessels with high level of accuracy. They comprise a system of two coupled Partial Differential Equations (PDEs), namely the mass and momentum conservation equations:

$$\frac{\partial a}{\partial t} + \frac{\partial (au)}{\partial x} = 0, \qquad \frac{\partial u}{\partial t} + u\frac{\partial u}{\partial x} = -\frac{1}{\rho}\frac{\partial p}{\partial x} \qquad (1)$$

where is the axial coordinate along the vessel, is the time, $a(x,\ t)$ is the luminal cross-sectional area, $u(x,\ t)$ is the cross-sectional average velocity in the axial direction, $p\ (x,\ t)$ is the average pressure and is the blood density. In this work, we neglect the effect of the wall shear stress.

Physics-Informed Neural Networks (PINNs) are neural networks comprising weights and biases that are tuned not just to fit data but also to comply with one or several PDEs. This is achieved by incorporating the residuals of the PDEs directly into the network's loss function. Other available equations related to the constitutive model, symmetry or periodicity constrains can also be included. As a result, optimizing this loss encourages the model's predictions to adhere to the conservation laws described by the PDEs. Furthermore, if extra data or additional physical constraints are available, they can be seamlessly integrated into the training process to further guide the network toward a physics-consistent solution.

We perform the study in an arterial network where in-silico *training* and *test* data of a healthy adult aorta are available via a numerical solver [4]. We assume the in-silico *training* data correspond to the *ground truth*, and proceed as if it was measured clinical data. The in-silico *training* dataset comprises the luminal area at those sections along the vessel's centreline at peak-systolic time t_{pks}, that is, $\mathcal{D}_a:\{\bigcup_{i=1}^{n_s} a_i(x_i,\ t\ =\ t_{pks})\}$, as well as the time evolution of the averaged velocity at a number n_s of sparsely sampled sections along each vessel, that is, $\mathcal{D}_u:\{\bigcup_{i=1}^{n_s} u^d(x_I, t^d)\}$, with n_d the number of samples in time. Figure 1 illustrates the in-silico velocity and area datapoints available data across the different branches of the thoracic network. This configuration is selected to align with the dataset presented in [2], where 4D-MRI was utilized to acquire densely sampled velocity data along the aorta, while area data was obtained solely at peak systole.

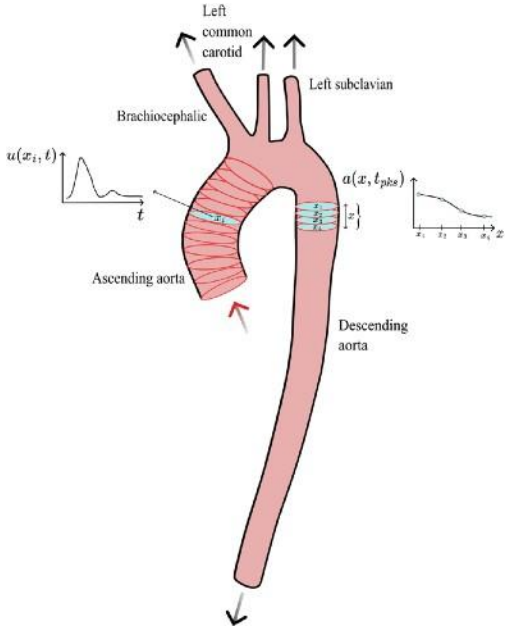

Figure 1: Thoracic aortic network with available training in-silico data of the time evolution of the velocity and the luminal area peak systolic datapoints, at different locations along the network. The discretization applied in the ascending aorta remains consistent across all subsequent branches, although not explicitly depicted in the Figure for brevity.

We proceed by training a PINN model for each vessel in the thoracic network to reconstruct $a(x,t)$ using only the PDE related to the conservation of mass, $PINN_{mass}$. The $PINN_{mass}$ loss function is expressed as follows:

$$\mathcal{L}^{mass} = \mathcal{L}^{mass}_{\mathcal{PDE}} + \mathcal{L}^{mass}_{data} + \mathcal{L}^{mass}_{cyclic} \tag{2}$$

Here, the PDE loss $(\mathcal{L}^{mass}_{\mathcal{PDE}})$ is given by:

$$\mathcal{L}^{mass}_{\mathcal{PDE}} = \frac{1}{n^{coll}} \sum_{j=1}^{n_{coll}} \left(\frac{\partial a}{\partial t}\bigg|_{(x_c^j, t_c^j)} + \frac{\partial (au)}{\partial x}\bigg|_{(x_c^j, t_c^j)} \right)^2 \tag{3}$$

where $(a, u) = PINN_{mass}(x, t; \boldsymbol{w}_{mass})$, n_{coll} represents the number of collocation points $(x_c,\ t_c)$ randomly sampled over the space-time domain defined by $x \in [x_o, x_f]$ and $t \in [t_o, T]$. Here, x_o and x_f are the positions of the initial and final sections of the vessel, t_o is the start time of the cardiac cycle, and is the total cardiac cycle duration. The data loss $\mathcal{L}^{mass}_{data}$ and cyclic loss $\mathcal{L}^{mass}_{cyclic}$ are defined as follows:

$$\mathcal{L}^{mass}_{data} = \sum_{i=1}^{n_s} \frac{1}{n_d} \sum_{d=1}^{n_d} \left(u(x_i, t^d) - u_i(x_i, t^d)\right)^2 + \sum_{i=1}^{n_s} \left(a(x_i, t_{pks}) - a_i(x_i, t_{pks})\right)^2 \tag{4}$$

$$\mathcal{L}^{mass}_{cyclic} = \frac{1}{n_{coll}} \sum_{j=1}^{n_{coll}} \left(a(x_c^j, t = t_o) - a(x_c^j, t = T)\right)^2 \tag{5}$$

where the cyclic loss $\mathcal{L}_{cyclic}^{mass}$ enforces periodicity in the inferred solution, and is a critical constraint due to the limited data available in the domain and the absence of boundary data. The configuration of a training step for the proposed PINN is illustrated in Figure 2.

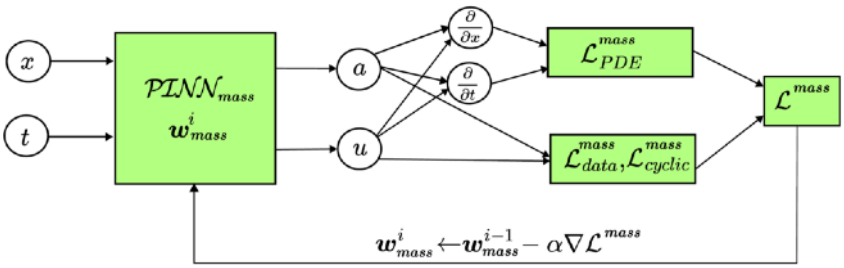

Figure 2: Illustration of a training step for the proposed $PINN_{mass}$, where α denotes the learning rate.

For the reconstruction of the pressure wave $p(x,t)$ and the vessel space-varying stiffness $K_o(x)$, we use the pretrained $PINN_{mass}$ to first obtain estimates of the velocity field and the luminal area and its derivatives. These are fed to a second decoupled PINN model, dubbed $PINN_{momentum}$, that runs parallel with the $PINN_{mass}$. Note that the parameters of the $PINN_{mass}$, $\boldsymbol{w}_{mass}$, do not vary across iterations now, they are static. Only the parameters of the $PINN_{momentum}$, $\boldsymbol{w}_{momentum}$ are adjusted throughout the learning. While the $PINN_{mass}$ was trained to ensure conservation of mass, the $PINN_{momentum}$ seeks to comply with the momentum equation. The loss for the $PINN_{momentum}$ is assembled in an equivalent way to the $PINN_{mass}$. For each vessel in the thoracic network, we aim to reconstruct $p(x,t)$ and $K_o(x,t)$ using only the PDE related to the conservation of momentum. The $PINN_{momentum}$ loss function is expressed as follows:

$$\mathcal{L}^{momentum} = \mathcal{L}_{\mathcal{PDE}}^{momentum} + \mathcal{L}_{data}^{momentum} + \mathcal{L}_{cyclic}^{momentum} \tag{6}$$

Here, the PDE loss $(\mathcal{L}_{\mathcal{PDE}}^{momentum})$ is given by:

$$\mathcal{L}_{\mathcal{PDE}}^{momentum} = \frac{1}{n^{coll}} \sum_{j=1}^{n_{coll}} \left(\frac{\partial u}{\partial t}\bigg|_{(x_c^j, t_c^j)} + u \frac{\partial u}{\partial x}\bigg|_{(x_c^j, t_c^j)} = -\frac{1}{\rho} \frac{\partial p}{\partial x}\bigg|_{(x_c^j, t_c^j)} \right)^2 \tag{7}$$

where $p(x,t) = p_s(x) + K_o(x,t_o)\left(\sqrt{\frac{a}{a_o}} - 1\right)$, $(a,u) = PINN_{mass}(x,t;\boldsymbol{w}_{mass})$, $(p, K_o) = PINN_{momentum}(x,t;\boldsymbol{w}_{momentum})$. The $\mathcal{L}_{data}^{momentum}$ and the $\mathcal{L}_{cyclic}^{momentum}$ are formulated in a similar way, but now the available data includes 3 additional datapoints corresponding to the diastolic pressure (p_d) and the systolic pressure (p_s) at the vessel's inlet section, hence

$$\mathcal{L}_{data}^{momentum} = (p(x_o,t_o) - p_d(x_o,t_o))^2 + \left(p(x_f,t_f) - p_d(x_o,t_f)\right)^2 + (p(x_o,t_{pks}) - p_s(x_o,t_{pks}))^2 \tag{8}$$

$$\mathcal{L}_{cyclic}^{momentum} = \frac{1}{n_{coll}} \sum_{j=1}^{n_{coll}} (K_o(x_c^j, t = t_o) - K_o(x_c^j, t = T))^2 \tag{9}$$

Figure 3 shows a representation of a training step of the $PINN_{mass}$ (green) coupled with the pretrained $PINN_{momentum}$ (yellow).

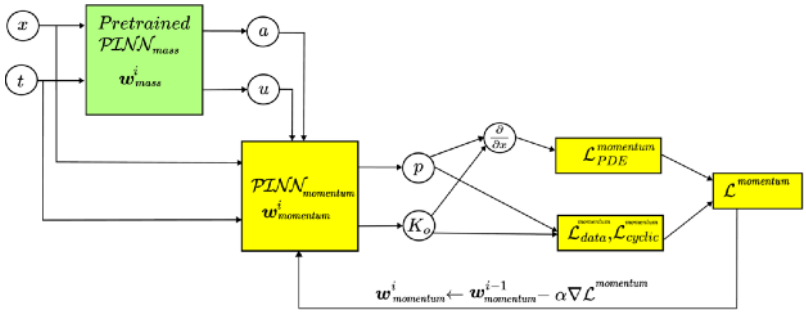

Figure 3: Illustration of a training step for the proposed $PINN_{momentum}$, where α denotes the learning rate.

3. Results

Figure 3 (a) shows the reconstructed area $a(x,\ t)$ over time at different sections of the AA, compared with in-silico *test* data. Figures 3 (b) and 3 (c) show the reconstructed area for the LSA and DA respectively. The rest of the vessels in the network (BCA, LCCA) also show similar results (not depicted for brevity). Notice red points indicating peak systolic luminal area datapoints at the different sections. These are, together with the velocity time evolution at those locations, the only data provided to the $PINN_{mass}$ for inferring the space and time variation of the area. Results are in agreement with in-silico data. Importantly, the reconstruction is particularly accurate at initial time t_o, meaning that the diastolic geometry is successfully retrieved. Relative RMSE errors are lower than 2% .

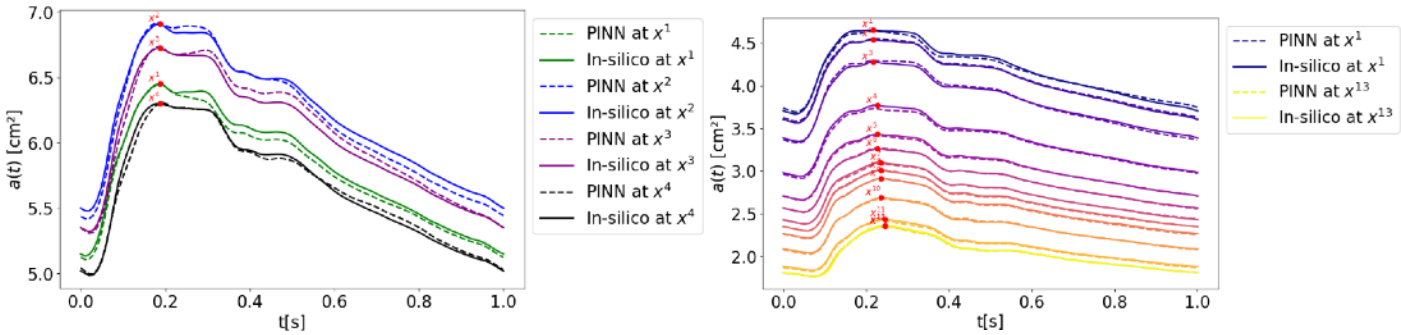

Figure 4: (a) $PINN_{mass}$ reconstruction of the luminal area in time, at several location of the AA, compared with in-silico test data. Red points correspond to peak systolic, and are fed $PINN_{mass}$ algorithm. (b) Reconstruction for the LSA. (c) Reconstruction for the DA.

Figure 4 (a) shows the fitted velocity $u(x,\ t)$ over time at different sections of the AA. Figures 4 (b) and 4 (c) show the fitted velocity for the LSA and DA, respectively. The rest of the vessels in the network (BCA, LCCA) also show similar results (not depicted for brevity). PINN fitting is almost undistinguishable from provided with in-silico *training* data. Relative RMSE errors are lower than 1% .

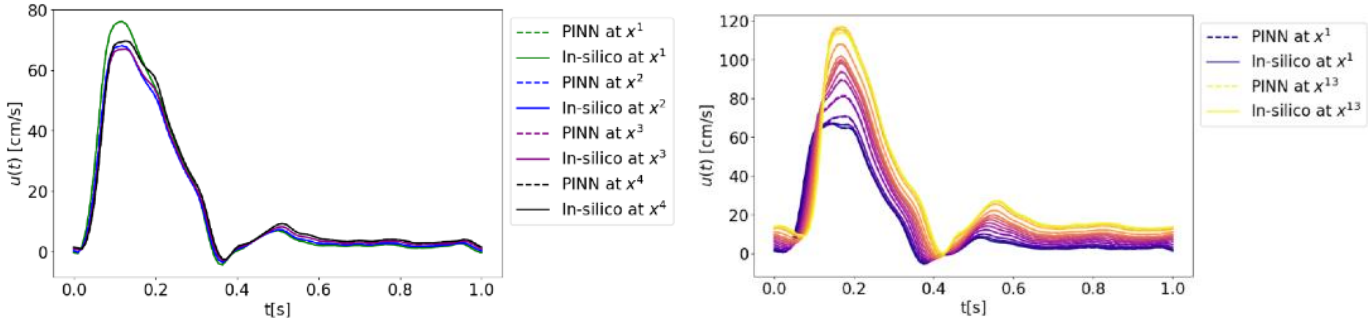

Figure 5: (a) $PINN_{mass}$ reconstruction of fitted velocity in time, at several location of the AA, compared with in-silico test data. (b) Fitted velocity for the LSA. (c) Fitted velocity for the DA.

Finally, Figure 6 (a) shows the reconstructed pressure $p(x,t)$ over time at different sections of the AA, compared with in-silico *test* data. Figure 6 (b) shows the reconstructed space-varying stiffness $K_o(x)$ for the AA. Red points indicate diastolic and systolic pressure reference datapoints only available at vessel's inlet section. These datapoints are fed to the $PINN_{momentum}$ for inferring the space and time variation of the pressure and the space variation of the stiffness. Results for the pressure reconstruction are in close agreement with in-silico test data, with relative RMSE errors lower than 3%. For the reconstruction of $K_o(x)$, it is observed that the $PINN_{momentum}$ is able to retrieve a variation with the space that was not accounted for when generating the in-silico training data, where a constant value of $c_o(x) = 4.56\ m/s$ was assumed, hence $K_o(x) = const$. The data-driven discovery of the space variation of $K_o(x)$ is therefore not decisive in this example, but it will prove much useful when tackling scenarios where the stiffness of the vessel can vary significantly, i.e. due to aneurysms, arteriosclerosis, etc, where no clinical measurements of the vessel's stiffness can be performed.

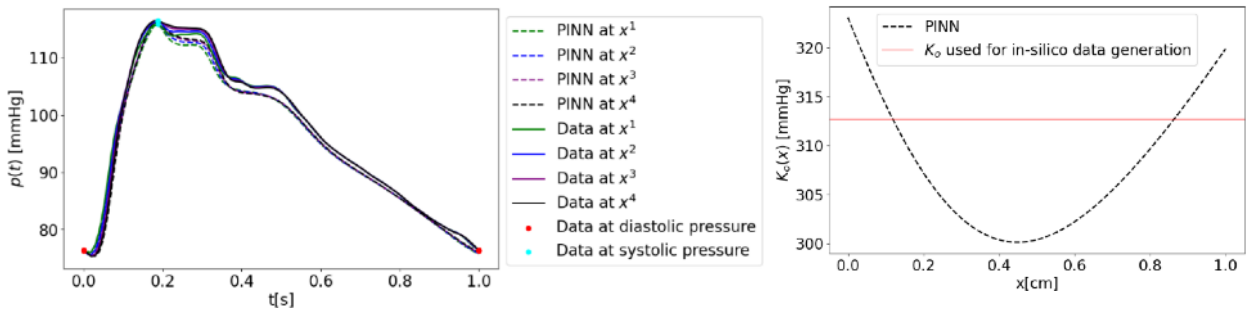

Figure 6: (a) $PINN_{momentum}$ reconstruction of pressure in time, at several location of the AA, compared with in-silico test data. Red points indicate diastolic pressure datapoints, and blue point indicates systolic pressure datapoint, given as training data. (b) $PINN_{momentum}$ reconstruction of the space-varying stiffness $K_o(x)$ for the AA.

6. Conclusions and future work

In this work, we propose two different architectures to retrieve luminal area, pressure and vessel stiffness from a sparse in-silico velocity training dataset, obtaining good agreement between the PINN reconstructions and the generated test in-silico dataset. Next steps include applying the same methodology using experimental MRI data provided in the same work [1], instead of in-silico data. In that case, measurements of the velocity and the luminal area are even sparser in space (only one location along AA and 4 locations along DA), but their evolution in time is available.

Acknowledgements

This work was supported by project PID2023-150074NB-I00 funded by the MICIU/AEI/ 10.13039/501100011033/ and from the European Union ''NextGenerationEU/PRTR''.

References

[1] Alastruey, J., Xiao, N., Fok, H., Schaeffter, T., & Figueroa, C. A. (2016). On the impact of modelling assumptions in multi-scale, subject-specific models of aortic haemodynamics. *Journal of The Royal Society Interface*, *13*(119), 20160073.

[3] de Vecchi A, Faraci A, Fernandes JF, Marlevi D, Bellsham-Revell H, Hussain T, Laji N, Rui jsink B, Wong J, Razavi R, Anderson D, Salih C, Pushparajah K, Nordsletten D, Lamata P. Unlocking the Non-invasive Assessment of Conduit and

Reservoir Function in the Aorta: The Obstructive Descending Aorta in HLHS. J Cardiovasc Transl Res. 2022 Oct;15(5):1075-1085. doi: 10.1007/s12265-022-10221-4.

[2] Raissi, M., Perdikaris, P., & Karniadakis, G. E. (2019). Physics-informed neural networks: A deep learning framework for solving forward and inverse problems involving nonlinear partial differential equations. *Journal of Computational physics*, *378*, 686-707.

[4] Murillo, J., Navas-Montilla, A., & García-Navarro, P. (2019). Formulation of exactly balanced solvers for blood flow in elastic vessels and their application to collapsed states. *Computers & Fluids*, *186*, 74-98.

[5] Murillo, J., & García-Navarro, P. (2023). Numerical coupling of 0D and 1D models in networks of vessels including transonic flow conditions. Application to short-term transient and stationary hemodynamic simulation of postural changes. *International Journal for Numerical Methods in Biomedical Engineering*, *39*(11), e3751.